Multifunctional solid/solid phononic crystal

N. Swinteck, Jerome O. Vasseur, Anne-Christine Hladky, Charles Croënne, S. Bringuier, P.A. Deymier

Multifunctional solid/solid phononic crystal

Cite as: J. Appl. Phys. **112**, 024514 (2012); https://doi.org/10.1063/1.4739264
Submitted: 10 January 2012 • Accepted: 27 June 2012 • Published Online: 24 July 2012

N. Swinteck, J. O. Vasseur, A. C. Hladky-Hennion, et al.

Multifunctional solid/solid phononic crystal

N. Swinteck,[1] J. O. Vasseur,[2] A. C. Hladky-Hennion,[2] C. Croënne,[3] S. Bringuier,[1] and P. A. Deymier[1]
[1]*Department of Materials Science and Engineering, University of Arizona, Tucson, Arizona 85721, USA*
[2]*Institut d'Electronique, de Micro-électronique et de Nanotechnologie, UMR CNRS 8520, Cité Scientifique, 59652 Villeneuve d'Ascq Cedex, France*
[3]*Department of Physics and Astronomy, University of Manitoba, Winnipeg, Manitoba R3T 2N2, Canada*

(Received 10 January 2012; accepted 27 June 2012; published online 24 July 2012)

A two-dimensional, solid/solid phononic crystal (PC) comprised a square array of steel cylinders in epoxy is shown to perform a variety of spectral, wave vector, and phase-space functions. Over a range of operating frequencies, the PC's elastic band structure shows uniquely shaped equifrequency contours that are only accessible to excitations of longitudinal polarization. Under this condition, the PC is shown to behave as (1) an acoustic wave collimator, (2) a defect-less wave guide, (3) a directional source for elastic waves, (4) an acoustic beam splitter, (5) a phase-control device, and (6) a *k*-space multiplexer. Wave vector diagrams and finite-difference time-domain simulations are employed to authenticate the above mentioned capabilities. © *2012 American Institute of Physics*. [http://dx.doi.org/10.1063/1.4739264]

I. INTRODUCTION

Composite structures comprised periodic arrangements of scatterers embedded in a host matrix material can strongly affect the propagation of classical waves such as electromagnetic waves, acoustic waves, and elastic waves. Composite materials that modulate the propagation characteristics of electromagnetic waves are classified as photonic crystals, whereas the term phononic crystal (PC) describes composites affecting acoustic wave propagation or elastic wave propagation. Since the first demonstration of a photonic crystal in 1987 (Ref. 1) (and subsequent demonstrations of PCs years later), the study of periodic media has exploded with popularity.

PCs come in one-dimensional (1D), two-dimensional (2D), and three-dimensional (3D) forms. 1D PCs consist of alternating layers or stacks of different elastic materials. 2D PCs are comprised periodic arrays of rod-like inclusions of one elastic material dispersed throughout a host matrix medium of a different elastic material. 3D PCs utilize lattice arrangements (simple cubic, body-centered cubic, face-centered cubic) of elastic scatterers of various geometries (spheres, cubes, etc.) dispersed throughout a dissimmilar host matrix material. The periodic nature of PCs allows for the modification of phonon dispersion via Bragg scattering, multiple scattering processes, and/or local resonances and offers a variety of properties such as spectral properties (ω-space), wave vector properties (*k*-space), and phase properties (φ-space).

Spectral properties result from gaps in the transmission spectra for stopping phonons. Sigalas and Economou first proved the existence of frequency gaps in the density of state and band structure for acoustic and elastic waves in the early 1990s.[2,3] Shortly after, the first full band structure calculation for vibrations of transverse polarization in a 2D, periodic elastic composite was reported.[4] In 2001, experimental and theoretical efforts demonstrated an absolute band gap for a 2D, solid/solid PC.[5] These findings led to the design of PCs with specific ω-space functions. For example, a PC with a channel of missing inclusions was shown to act as a waveguide to acoustic signals with frequency in the acoustic band gap.[6] Additionally, it was shown that a row of missing inclusions in a 2D PC can couple to an acoustic wave source to yield a resonant cavity capable of directing and amplifying acoustic energy.[7–11] Moreover, by exploiting narrow passing bands, PCs were designed to filter broadband acoustic signals.[12,13]

Wave vector properties result from passing bands with unique refractive characteristics, such as negative refraction or zero-angle refraction. Negative refraction is achieved when the wave group velocity (the direction of propagation of energy) is antiparallel to the wave vector. Bragg scattering in PCs results in band-folding whereby several bands with negative slope are produced, a prerequisite for negative refraction. A combined theoretical and experimental study of a 3D PC composed of tungsten carbide beads in water has shown the existence of a strongly anisotropic band with negative refraction.[13,14] A 2D PC constituted of a triangular lattice of steel rods immersed in a liquid exhibited negative refraction and was used to focus ultrasound.[15,16] High fidelity imaging is obtained when all-angle negative refraction conditions are met, that is, the equifrequency contour (EFC) of the PC is circular and matches the EFC of the medium in which it is embedded. A flat lens of this design achieved focusing and subwavelength imaging of acoustic waves.[17] A broader range of unusual refractive properties was also reported in a study of a PC consisting of a square array of cylindrical polyvinylchloride inclusions in air.[18] This crystal exhibits positive, negative, or zero refraction depending on the angle of the incident acoustic beam. Zero-angle refraction can lead to wave guiding/localization without defects. The unusual refraction in this crystal is highly anisotropic due to the square-like shape of its EFCs.

The extension of PC properties beyond ω-space and *k*-space and into the realm of acoustic wave phase-space

(φ-space) has recently been reported.[19–21] The concept of phase-control between propagating acoustic waves in a PC can be realized through analysis of its band structure and EFCs.[19,20] The dominant mechanisms behind the control of phase between propagating acoustic waves in 2D PCs arises from the anisotropy of the EFC, giving rise to non-collinear wave and group velocity vectors.

In this paper, we present a multifunctional 2D, solid/solid PC comprised a square array of steel cylinders in epoxy. In utilizing the spectral, wave vector, and phase properties, this PC exemplifies, we demonstrate the epoxy/steel PC behaving as (1) an acoustic wave collimator, (2) a defect-less wave guide, (3) a directional source for elastic waves, (4) an acoustic beam splitter, (5) a phase-control device, and (6) a k-space multiplexer. These capabilities highlight the unique ability of the PC to operate in ω-space, k-space, and φ-space. In Sec. II of this report, the epoxy/steel PC is described along with the models and numerical methods used to characterize its properties. In Sec. III, with wave vector diagrams and finite-difference time-domain (FDTD) simulations, we explain and demonstrate the above mentioned ω-space, k-space, and φ-space capabilities of the PC. Finally in Sec. IV, conclusions are drawn from the study.

II. MODEL AND NUMERICAL METHODS

The PC is a 2D composite structure consisting of a square array of steel inclusions (cylinders) embedded in a host matrix of epoxy. The spacing between the cylinders (of radius $r = 1.00$ mm) is $a = 3.23$ mm, owing to an inclusion filling fraction of 30%. The density, longitudinal speed of sound, and transverse speed of sound for epoxy are 1180 kg/m^3, 2535 m/s, and 1157 m/s, respectively. For steel, the parameters are 7780 kg/m^3, 5825 m/s, and 3227 m/s.

Spectral and wave vector properties for the infinite, periodic PC are evaluated using the plane wave expansion (PWE) method.[3] Spectral, wave vector, and phase properties for a finite slab of the PC are evaluated using the FDTD method.[22] For FDTD analysis, the PC slab is sandwiched between two homogeneous regions of material.

The elastic band structure and EFCs for the infinite, periodic PC are constructed using the PWE method. This numerical scheme replaces the elastic wave equation with an eigenvalue problem by taking the Fourier expansion of the elastic displacement field (and of the physical parameters of the constituent materials) along reciprocal lattice vectors. 441 reciprocal space vectors were utilized to ensure convergence of the method. The PWE rendering of the elastic band structure (band gap frequency range) is consistent with the transmission spectra found by the FDTD method to within a few kHz. Figure 1(a) shows the band structure of the infinite, periodic PC along the edges of the irreducible Brillouin zone (BZ). Only XY modes (vibrational modes with wave vector and displacement field belonging to the plane perpendicular to the inclusions) are reported. An absolute band gap is observed between 238 and 410 kHz. From 540 to 620 kHz, we observe a passing band with negative slope. Figure 1(b) shows the EFCs corresponding to this frequency range. The EFCs are centered on the Γ-point and have symmetry

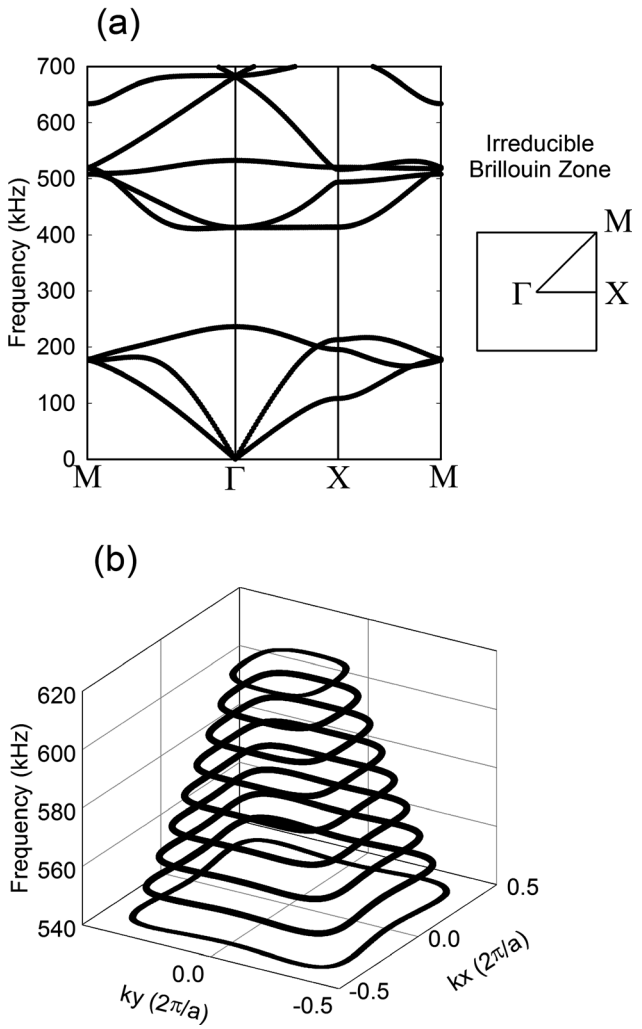

FIG. 1. (a) Band structure of the infinite, periodic epoxy/steel PC along high symmetry directions in the first BZ. (b) EFCs for epoxy/steel PC corresponding to the 7th band in (a). Collimating properties and zero-angle refraction are associated with the flatness of the sides of these square-like contours.

consistent with the ordering of the steel inclusions (square-like). In this frequency range, the near-perfect flatness of the sides of these square-like contours makes this PC unique because multiple Bloch waves exist with identical group velocity vectors. This feature is strongly exploited in later ω-space, k-space, and φ-space demonstrations involving acoustic wave collimation and phase manipulation of acoustic waves. In addition to their favorable shape, the EFCs are strictly accessible to excitations of longitudinal polarization (the 7th band in Figure 1(a) corresponds to a longitudinal, elastic mode). This is a unique and fortunate consequence because analyzing wave propagation in solids is typically difficult due to the fact that propagative modes of longitudinal polarization are superposed over propagative modes of transverse polarization. Discovering the conditions that determine the relative phase between propagating elastic waves in the epoxy/steel PC is straightforward when the modes of vibration are decoupled. In slightly more complex scenarios (circumstances where longitudinal and transverse modes simultaneously exist), the conditions for phase manipulation of acoustic/elastic waves can be revealed as well.

FDTD simulations shed light on several capabilities of the PC. In the FDTD method, a simulation space is constructed of a grid of mesh points. Each mesh point represents a material and is associated with a density and certain set of material specific elastic parameters. Large FDTD simulation meshes can be designed to model intricate, bulk systems by appropriately defining each mesh point with the correct material parameters. Specifically for this study, the FDTD grid will be designed to model a 2D slab of the epoxy/steel PC sandwiched between two regions of homogeneous material. The homogeneous regions may be solid or fluid. To use the FDTD method to simulate fluids, one approximates the fluid as a solid with transverse speed of sound (c_t) set equal to zero ($C_{44} = \rho c_t^2 = 0$). Over the entire FDTD grid, the elastic wave equation is discretized in time and space. Equation (1) shows a balance of linear momentum for a material without the addition of a body force term. u_m is the mth component of the displacement vector $\boldsymbol{u(r)}$, σ_{mk} are the elements of the stress tensor and $\rho(\boldsymbol{r})$ is density. The stress-strain relationship for an isotropic, linear elastic material is shown by Eq. (2). $\lambda(\boldsymbol{r})$ and $\mu(\boldsymbol{r})$ are the so-called Lamé coefficients, ε represents the strain tensor, and δ_{mk} is Kronecker's delta. The components of the strain tensor in Eq. (2) are related to the components of the displacement field by Eq. (3)

$$\frac{\partial^2 u_m}{\partial t^2} = \frac{1}{\rho}\frac{\partial \sigma_{mk}}{\partial x_k}, \tag{1}$$

$$\sigma_{mk} = \lambda \delta_{mk} \varepsilon_{jj} + 2\mu \varepsilon_{mk}, \tag{2}$$

$$\varepsilon_{mk} = \frac{1}{2}\left(\frac{\partial u_m}{\partial x_k} + \frac{\partial u_k}{\partial x_m}\right). \tag{3}$$

FDTD simulations are run for times between 0.1 and 0.5 ms with temporal discretization $\Delta t = 1.96 \times 10^{-9}$ s and spatial discretization $\Delta x = \Delta y = a/50$. At each time step, from spatial derivatives, the divergence of the stress tensor is calculated which allows for the iterative update of the displacement field. To perturb the FDTD mesh at each time step, a wave emitting source is placed somewhere on the FDTD grid. The source consists of a line of grid points that are displaced orthogonally with respect to the source line sinusoidally in time. To close the simulation space along the mesh edge, first order Mur absorbing boundary conditions are employed to avoid wave reflections.[23] To characterize wave propagation in solid regions, we report FDTD displacement fields to differentiate between longitudinal and transverse waves. To characterize wave propagation in fluid regions, we introduce two scalar metrics, subsequently referred to as pressure (P) and average pressure (P'). From Eq. (2), P is defined as minus the trace of the stress tensor. An instantaneous pressure field for a given FDTD simulation is found by calculating P over all grid points in the FDTD mesh at one time step. We define P' as the time average of the absolute value of P over some time interval

$$P = -\Big((\lambda + 2\mu)\varepsilon_{11} + \lambda\varepsilon_{22} + \lambda\varepsilon_{11} + (\lambda + 2\mu)\varepsilon_{22}\Big),$$

$$P' = \frac{1}{T}\int_{t_o}^{t_o+T} |P(t')|\, dt'.$$

For this study the time interval is the period (T) of one wave cycle from the oscillating line source in the FDTD simulation mesh. P' is useful because it assigns a scalar value to the temporal evolution of pressure at a given point in the FDTD mesh. P' is used to characterize phase relationships between propagating acoustic waves.

III. RESULTS

A. Zero-angle refraction, defect-less waveguiding, and a directional source for elastic waves

Due to the square-like shape of its EFCs, the epoxy/steel PC exhibits exceptional k-space features between 540 and 620 kHz. Collimating properties and zero-angle refraction are associated with the flatness of the sides of these square-like contours. To demonstrate these properties, we utilize a series of wave vector diagrams and FDTD simulations. To begin with, we direct the reader to Figure 2 to outline the configuration used in our first FDTD demonstration. Figures such as this are particularly helpful for understanding wave

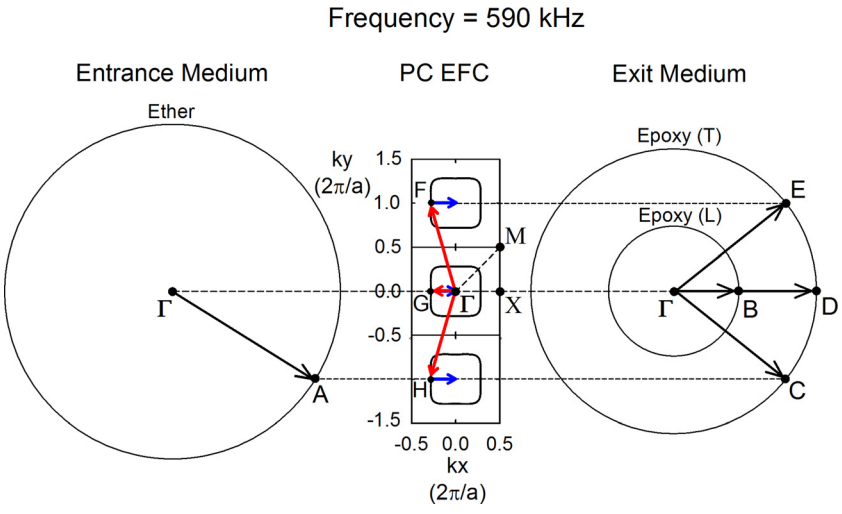

FIG. 2. (Center) An extended zone scheme representation of the first BZ for the epoxy/steel PC at 590 kHz. (Left) A circular EFC representing acoustic waves in ether. (Right) Two circular EFCs representing longitudinal, elastic and transverse, elastic waves in epoxy. Impinging wave vector ΓA excites periodic Bloch modes (ΓF, ΓG, and ΓH) in the PC k-space. These modes coincide with four excitations in homogeneous epoxy: one longitudinal (ΓB) and three transverse (ΓC, ΓD, and ΓE).

propagation through PCs. The scheme described in Section II applies to this figure—a slab of the epoxy/steel PC is sandwiched between two regions of homogeneous material, an entrance region and an exit region. Generally, the figure describes a wave launched from some entrance medium at the PC surface. The wave propagates through the PC and exits into some exit medium. Pictured in the center of Figure 2 is an extended zone scheme representation of the PC's first BZ with square-like EFCs corresponding to 590 kHz waves. The irreducible BZ (ΓXM) matches that shown in Figure 1(a). On the left, we see an EFC representing acoustic waves in ether. On the right, we see two EFCs describing longitudinal, elastic waves, and transverse, elastic waves in epoxy. Figure 2 specifically shows (1) how traveling waves refract at different interfaces (e.g., the ether-PC interface and the PC-epoxy interface) and (2) how propagative longitudinal modes convert into propagative transverse modes. Consider an acoustic wave in ether impinging upon the PC surface with wave vector ΓA (Figure 2). Ether is chosen as the entrance medium due to its much lower longitudinal speed of sound compared to epoxy ($c_{L,ether} = 985$ m/s). At the interface between ether k-space and the PC k-space, the k_y component of ΓA is conserved. Several Bloch waves with this wave vector component (plus/minus multiple translations of a reciprocal lattice vector) are excited in the PC k-space. These modes are longitudinal, elastic modes, and are detailed in Figure 2 with wave vectors ΓF, ΓG, and ΓH. The arrows orthogonal to the square-like EFCs represent group velocity vectors (blue arrows in Figure 2). The incident wave propagates from the left to the right in the PC with energy following a path consistent with the group velocity vector. At the boundary between the PC and the exit medium (epoxy), the k_y component of each excited Bloch wave vector in the PC is conserved again. This excites specific modes in the epoxy medium: one longitudinal (ΓB) and three transverse (ΓC, ΓD, and ΓE). The longitudinal mode and transverse mode (ΓD) leave the PC with phase and group velocity vectors perpendicular to the PC-epoxy interface (zero-angle refraction). The ΓC and ΓE transverse modes represent negative and positive refraction, respectively, at the PC-epoxy interface. From here, we desire to characterize the waves leaving the backside of the PC with FDTD displacement field calculations. Figures 3(a) and 3(b) show the u_x and u_y displacement fields, respectively, for a 590 kHz acoustic wave in ether impinging upon the epoxy/steel PC surface. The ether-PC interface (ether on left, PC on right) occurs at the 45 mm mark along the horizontal axis of Figures 3(a) and 3(b). The PC-epoxy interface occurs at the 105 mm mark. The acoustic wave enters the middle of the PC at an incidence angle corresponding to −32°. We observe zero-angle refraction of the wave at the ether-PC interface, which is consistent with the direction of the group velocity vectors in Figure 2. Inside the PC, wave energy is spatially restricted to a well-defined volume. At the interface between the PC and epoxy, we observe three exiting modes consistent with the wave vectors ΓB, ΓC, and ΓE of Figure 2. The u_x displacement field in Figure 3(a) indicates two transverse waves leaving the back side of the PC at −38° and +38° (wave vectors ΓC and ΓE, respectively). The u_y displacement field in Figure 3(b) shows an additional exiting

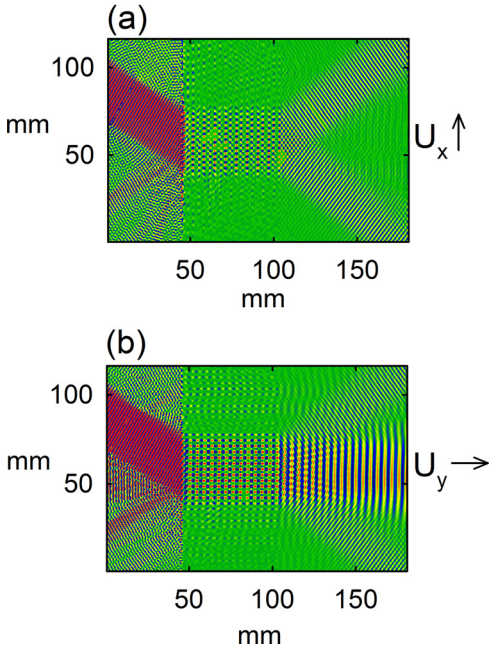

FIG. 3. (a) and (b) FDTD displacement field calculation of an acoustic wave in ether impinging upon the PC surface at 590 kHz. Zero-angle refraction occurs at the interface between ether and the PC (45 mm mark along horizontal axis). Wave energy is spatially restricted to a well-defined volume inside the PC. At the interface between the PC and exit epoxy medium (105 mm mark along horizontal axis), two transverse modes exit at ±38° (a) and one longitudinal mode exits at 0° (b).

wave, longitudinal mode ΓB leaving at 0°. The longitudinal mode is more intense than the two transverse waves; this is strictly due to mode conversion at the PC-epoxy interface. In the case of the third transverse mode (ΓD of Figure 2), longitudinal-to-transverse mode conversion at the PC-epoxy interface is weak, therefore, we observe zero transmission for ΓD in Figure 3(a). To remark on the abilities of the epoxy/steel PC, we call attention to fact that zero-angle refraction is observed at two distinct interfaces (the ether-PC interface and the PC-epoxy interface) for propagating waves of longitudinal polarization. This unusual happening allows input acoustic signals in ether to be maintained throughout the PC and exit epoxy medium. Behavior similar to this occurs for several impinging acoustic waves within a wide solid angle. For 590 kHz impinging acoustic waves in ether, the epoxy/steel PC collimates waves with the following incidence angles: −38° to −25°, −5.5° to +5.5°, +25° to +38°. These acoustic waves undergo zero-angle refraction at the ether-PC interface and convert into longitudinal, elastic modes in the exit epoxy medium. Impinging waves with angles outside, these limits will either be positively/negatively refracted due to curvature of the EFC or will undergo total-reflection at the ether-PC interface.

We elaborate on the capacity of the epoxy/steel PC to spatially restrict wave energy by comparing the previous scheme to a PC waveguide structure. PC waveguides are fundamentally perfect structures for controlling wave travel because propagating waves can only couple to accessible waveguide modes. This spatially restricts wave energy to the channel of defects in the PC waveguide. The waveguide we consider is a slab of the epoxy/steel PC with a straight

channel of missing steel inclusions. The waveguide has the same thickness as the PC used in Figures 3(a) and 3(b) and is sandwiched between two homogeneous regions of material—ether on the left and epoxy on the right. The width of the channel in the waveguide is comparable to the width of the beam propagating through the PC in Figures 3(a) and 3(b)—specifically; the width of the beam propagating through the PC in Figures 3(a) and 3(b) is 15 λ, where λ is the wavelength of the acoustic energy emanating from the source in ether. For comparison purposes, the wave launched at the waveguide will be an acoustic wave in ether with incidence angle -32°. The wave enters the waveguide at the center of the channel. A FDTD displacement field calculation is reported to disclose information on the quality of the guide and the ability of the waveguide structure to restrict beam divergence after elastic wave energy exits the PC waveguide. Figures 4(a) and 4(b) show displacement field calculations (u_x and u_y, respectively) for a 320 kHz acoustic wave in ether impinging upon the waveguide structure. 320 kHz is selected as the operating frequency because it corresponds to the middle of the PC band gap (see Figure 1(a)). At the interface between ether and the opening of the waveguide (45 mm mark along the horizontal axis), we observe a conversion of modes; the impinging acoustic wave in ether couples to accessible waveguide modes. These waveguide excitations undergo multiple reflections with the walls of the waveguide and subsequently exit the PC waveguide structure. Figures 4(a) and 4(b) show highly diffuse displacement fields on the backside of the PC waveguide. Where the waveguide structure is present, elastic wave

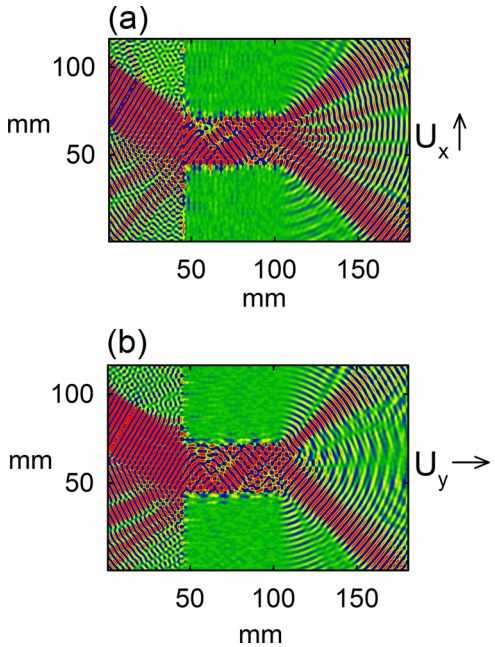

FIG. 4. (a) and (b) FDTD displacement field calculation. An impinging acoustic wave in ether strikes the surface of a PC waveguide structure at -32°. The waveguide structure is composed of an epoxy/steel PC slab with several rows of missing steel inclusions. Impinging acoustic energy couples to accessible waveguide modes. Waveguide excitations undergo several reflections with the bounds of the waveguide. Upon exiting the waveguide, a highly diffuse displacement field is apparent on the backside of the structure.

energy is contained within the bounds of the waveguide. Where the waveguide structure is missing, elastic wave energy spreads. For PC waveguides, the guiding of wave energy ceases once the waveguide is removed. In instances where spatial restriction of elastic wave energy in needed, it appears that the structure from Figures 3(a) and 3(b) is more desirable than the structure from Figures 4(a) and 4(b). As such, the epoxy/steel PC operates as a defect-less waveguide. With certainty, the refractive properties of the epoxy/steel PC prove to be more useful than the channeling properties of the PC waveguide in maintaining spatially restricted elastic wave energy. We add to the PC functions seen above. Here, instead of exciting Bloch modes in the PC k-space with an external wave stimulus (as was the case with impinging acoustic waves in ether), we place an elastic wave emitting source directly inside the PC between two columns of inclusions. Adjacent to the PC structure is a homogeneous region of epoxy where FDTD displacement field calculations are made. In the PC, the source oscillates in a manner that directs longitudinal, elastic waves parallel to the rows of steel inclusions. The source is constrained to oscillate at two frequencies of interest, the lower and upper limits of the follow frequency range: 540–620 kHz (see Figure 1(b)). The objective of this setup is to show (1) that exiting transverse excitations leave the backside of the PC at angles dependent upon the frequency of the oscillating line source inside the PC and (2) that exiting longitudinal excitations always undergo zero-angle refraction at the PC-epoxy interface no matter what the operating frequency. Ultimately, by exploiting the notion that this configuration offers decoupled longitudinal and transverse excitations in epoxy, one can view this set-up as a source for longitudinal/transverse elastic waves. We direct the reader to Figure 5 to elaborate upon this assertion. In the center of Figure 5, we see an extended zone scheme representation of the PC's first BZ with EFCs corresponding to 540 kHz waves (large, blue contour) and 620 kHz waves (small, red contour). On the left hand side, we see two circular contours for longitudinal, elastic waves in epoxy. The inner circle represents 540 kHz and the outer circle represents 620 kHz. On the right hand side, we see two sets of circular contours. One set represents longitudinal, elastic waves in epoxy (inner circle is 540 kHz, outer circle is 620 kHz). The other represents transverse, elastic waves in epoxy (inner circle is 540 kHz, outer circle is 620 kHz). Wave vectors ΓA and $\Gamma A'$ describe waves emanating from the 540 and 620 kHz embedded line sources, respectively. These stimuli coincide with multiple Bloch excitations inside the PC k-space. ΓA is linked to the 540 kHz Bloch excitations (ΓE, ΓF, and ΓG). $\Gamma A'$ is linked to the 620 kHz Bloch excitations ($\Gamma E'$, $\Gamma F'$, and $\Gamma G'$). For both frequencies, all Bloch modes associate with zero-angle refraction—group velocity vectors point in a direction perpendicular to the EFC (group velocity vectors not pictured in Figure 5). Wave energy from the embedded, oscillating line source travels through the PC and reaches the PC-epoxy interface. The k_y component of each Bloch wave excitation is conserved at the interface and this excites longitudinal and transverse modes in the exit epoxy medium. For 540 kHz, there is a longitudinal wave (ΓB) exiting at 0° (zero-angle refraction) and two

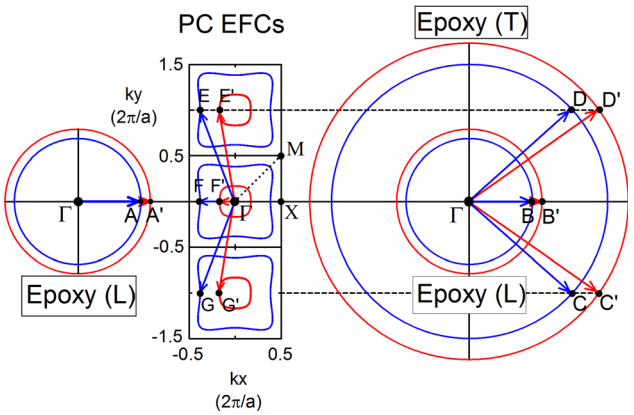

FIG. 5. (Center) An extended zone scheme representation of the first BZ for the epoxy/steel PC. PC EFCs are shown at 540 kHz (large, blue contour) and 620 kHz (small, red contour). To the left are two circular EFCs representing longitudinal, elastic waves in epoxy. The small, blue contour represents 540 kHz and the large, red contour represents 620 kHz. On the right are two sets of circular EFCs. One set represents longitudinal, elastic waves in epoxy (inner circle = 540 kHz, outer circle = 620 kHz). The other represents transverse, elastic waves in epoxy (inner circle = 540 kHz, outer circle = 620 kHz). For 540 kHz and 620 kHz (respectively), incident wave vectors ΓA and ΓA′ associate with distinct Bloch wave excitations in the PC *k*-space; ΓA excites ΓE, ΓF, and ΓG and ΓA′ excites ΓE′, ΓF′, and ΓG′. The 540 kHz and 620 kHz Bloch modes translate into two sets of wave excitations in epoxy. The 540 kHz set consists of a longitudinal wave (ΓB) exiting at 0° (zero-angle refraction) and two transverse waves (ΓC and ΓD) exiting at −42° and +42°, respectively. The 620 kHz set consists of a longitudinal wave (ΓB′) exiting at 0° (zero-angle refraction) and two transverse waves (ΓC′ and ΓD′) exiting at −34° and +34°, respectively. Exiting transverse excitations leave the backside of the PC at angles dependent on frequency. Exiting longitudinal excitations always undergo zero-angle refraction at the PC-epoxy interface no matter what the operating frequency.

transverse waves (ΓC and ΓD) exiting at −42° and +42°, respectively. For 620 kHz, there is a longitudinal wave (ΓB′) exiting at 0° (zero-angle refraction) and two transverse waves (ΓC′ and ΓD′) exiting at −34° and +34°, respectively. With knowledge of the results of Figures 3(a) and 3(b), we do not anticipate any transverse excitations leaving the backside of the PC at 0°. We now use FDTD u_x displacement field calculations to verify that changing the operating frequency of the embedded, oscillating line source modifies the exit angle for transverse excitations. Figures 6(a) and 6(b) show the 540 and 620 kHz line sources oscillating inside the epoxy/steel PC, respectively. In both figures, the PC-epoxy interface occurs at the 45 mm mark along the horizontal axis. In Figure 6(a), we see two transverse excitations leaving the backside of the PC at angles consistent with those predicted by Figure 5 (±42°). Similarly, in Figure 6(b), we see transverse excitations exiting at ±34°. By modulating the frequency of the embedded, oscillating line source inside the PC, the angle at which transverse excitations leave the backside of the PC is varied. Opposite to this result, as Figure 5 proves, exiting longitudinal modes always undergo zero-angle refraction at the PC-epoxy interface regardless of operating frequency. Propagating longitudinal modes are decoupled from transverse excitations due to weak longitudinal-to-transverse mode conversion at the PC-epoxy interface for transverse excitations exiting at 0°. Ultimately, this configuration offers a scheme for isolated longitudinal, elastic and transverse, elastic waves in epoxy.

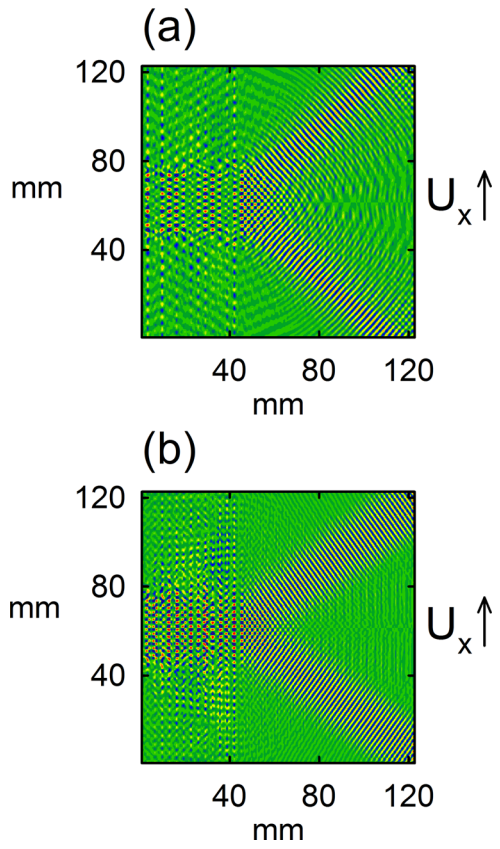

FIG. 6. FDTD u_x displacement field calculations for 540 kHz (a) and 620 kHz (b). In (a) and (b), an oscillating line source is embedded inside the epoxy/steel PC. The line source directs longitudinal, elastic waves in the *y*-direction. In (a), exiting transverse waves leave the backside of the PC at −42° and +42°. In (b), exiting transverse waves leave the backside of the PC at −34° and +34°.

B. Acoustic beam splitter and phase-control device

This sub-section remarks on (1) the splitting of an input acoustic signal into multiple signals through the use of the epoxy/steel PC and on (2) utilizing the epoxy/steel PC as a phase-control device for manipulating acoustic wave propagation. Here, the PC slab is sandwiched between two regions of water. We first demonstrate that an acoustic wave in water impinging upon the PC surface is split into several beams upon exiting the crystal. This notion can be understood by referring to Figure 7. An extended zone scheme representation of the PC's first BZ with square-like EFCs corresponding to 590 kHz waves is pictured in the center. The circles on the left and right hand sides represent the EFCs of 590 kHz acoustic waves in water. The wave vector of an acoustic wave in water impinging upon the PC surface is shown in the left hand circle (ΓA). The k_y component of ΓA is conserved at the interface between water *k*-space and the PC *k*-space, which excites several propagative modes in the PC (longitudinal elastic modes ΓE, ΓF, and ΓG). Each excited Bloch mode coincides with a group velocity vector that is perpendicular to the EFC (zero-angle refraction). The energy of the input acoustic signal travels from the left to the right inside the PC. At the PC-water interface, the k_y component of each Bloch excitation is conserved. These wave vector components coincide with the circular EFC of water on the

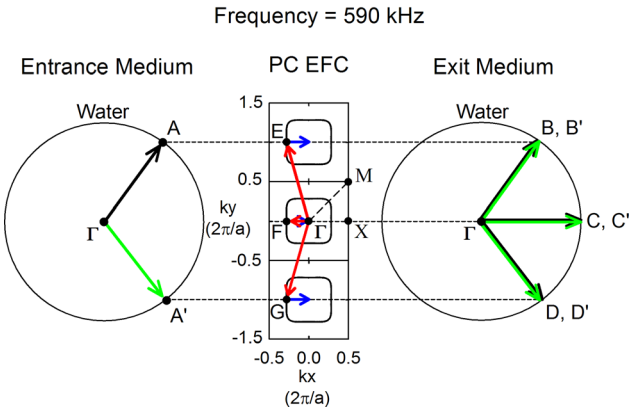

FIG. 7. (Center) Extended zone scheme representation of first BZ along with PC EFCs corresponding to 590 kHz. (Left and right) EFCs corresponding to 590 kHz acoustic waves in water. Wave vectors ΓA and ΓA′ impinge upon the surface of the PC at +52.3° and −52.3°, respectively. Identical Bloch modes are excited in the PC *k*-space. The k_y component of these excitations is conserved at the interface between the PC and exit water medium, resulting in six acoustic excitations in water: ΓB, ΓB′, ΓC, ΓC′, ΓD, and ΓD′. Because ΓA and ΓA′ share identical Bloch modes in the PC, ΓB = ΓB′, ΓC = ΓC′, and ΓD = ΓD′. ΓA and ΓA′ are called complementary angle inputs.

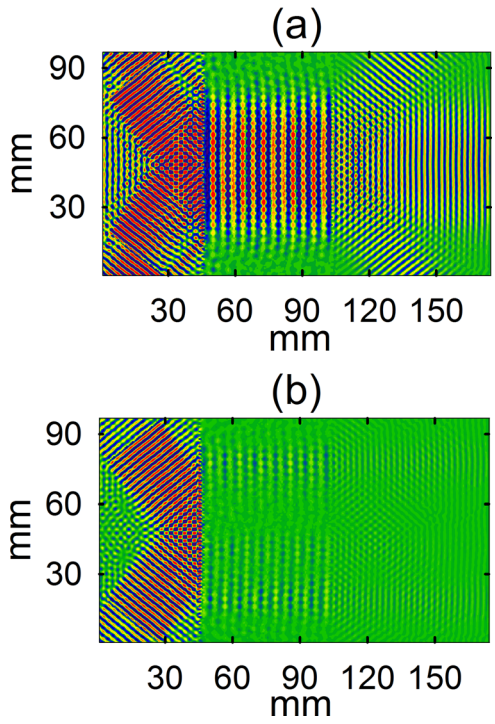

FIG. 8. (a) and (b) FDTD simulation (instantaneous pressure field (P)). Two acoustic waves (complementary angle inputs) in water impinge upon the PC surface at +52.3° and −52.3°. In (a), the acoustic sources oscillate in-phase and excite identical Bloch modes in the PC *k*-space. Bloch waves constructively interfere, contributing to intense acoustic pressure fields inside and outside the PC. On the backside of the PC, beam splitting is observed. In (b), the acoustic sources oscillate π radians out-of-phase. Bloch excitations destructively interfere inside the PC resulting in a near-zero pressure field on the backside of the crystal.

exit side of the PC and three acoustic wave modes result (ΓB, ΓC, and ΓD). The PC therefore splits an incident acoustic wave into three acoustic waves. We note, due to the symmetry of *k*-space, that an impinging acoustic wave with wave vector ΓA′ will excite the same Bloch modes as input wave vector ΓA. Because the two waves share identical Bloch modes inside the PC, they will excite identical exit modes in the water medium (ΓB = ΓB′, ΓC = ΓC′, ΓD = ΓD′). These acoustic inputs (ΓA and ΓA′) are subsequently referred to as complementary angle inputs. Figure 8(a)), an FDTD simulation mapping instantaneous pressure (*P*), shows two complementary angle inputs. The acoustic sources (located on the left hand side of the simulation) are in water and are angled at +52.3° and −52.3°. The sources oscillate in-phase with each other and enter the PC at precisely the same location. In Figure 8(a), we observe a region of intense pressure inside the PC. This is indicative of constructive interference between superposed Bloch modes. Upon exiting the crystal, we see three intense, well-defined acoustic beams—one exiting at +52.3°, one exiting at −52.3° and one exiting normal to the PC surface (0°). This image well-represents wave propagation detailed Figure 7. If the relative phase between the complementary angle inputs is adjusted such that the sources oscillate π-radians out-of-phase (Figure 8(b)), then destructive interference occurs between propagating Bloch excitations inside the PC and opposing wave amplitudes annihilate each other to yield a near-zero pressure field on the backside of the PC. Cancellation is not total because at the ends of each acoustic source there is slight divergence of acoustic energy leading to the excitation of additional Bloch modes in the PC *k*-space, which contributes to the non-zero pressure field on the exit side of the PC. Similar to the air/solid PCs used in Refs. 19 and 20, this *φ*-space function is wholly enabled by *k*-space symmetry. On the contrary to that shown in the aforementioned publications, this is the first ever demonstration of phase-control between propagating acoustic waves with a completely solid PC.

C. k-space multiplexing

Multiplexing is a method by which a superposition of signals (waves) is transported across the same supporting medium. The signals or waves differ in some characteristic feature. Typically, the characteristic feature is wave length, such as that seen in frequency-division multiplexing. In this section, we demonstrate a less familiar form of multiplexing by utilizing a signal's wave vector. This demonstration is subsequently called *k*-space multiplexing.

We slightly modify Figure 7 of Sec. III B to introduce the epoxy/steel PC behaving as a wave vector (*k*-space) multiplexer (see Figure 9). Two acoustic waves in water at two distinct angles of incidence impinge upon the epoxy/steel PC. The unique wave vector components of these excitations associate with distinct Bloch wave excitations in the PC *k*-space. In Figure 9, we observe that a specific set of Bloch wave vectors associate with the ΓA excitation (red arrows in PC *k*-space) and a different set of wave vectors correlate with the ΓA′ excitation (dark green arrows in PC *k*-space). Common to all excited Bloch modes is group velocity; for all excitations in the PC *k*-space, the direction in which energy propagates is orthogonal to the EFC (blue arrows denote zero-angle refraction). The input wave vectors (ΓA and ΓA′) have been multiplexed. Wave energy propagates

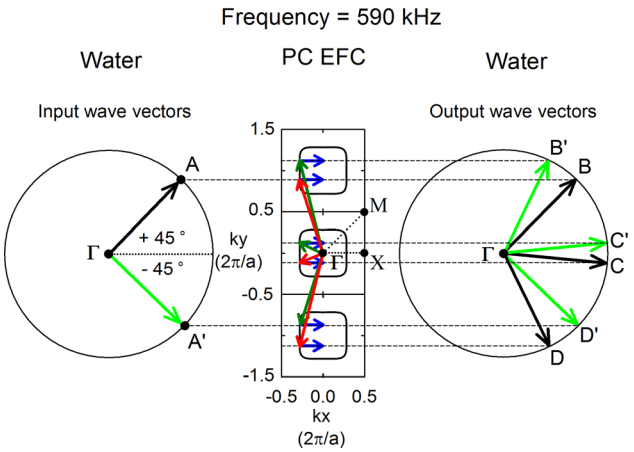

FIG. 9. (Center) extended zone scheme representation of first BZ along with PC EFCs corresponding to 590 kHz. (Left and right) circular EFCs corresponding to 590 kHz acoustic waves in water. Wave vectors ΓA and ΓA′ impinge upon the surface of the PC at +45° and −45°, respectively. In the PC *k*-space, a unique set of Bloch modes are excited due to ΓA (red arrows in PC *k*-space) and a different, unique set of Bloch modes are excited due to ΓA′ (dark green arrows in PC *k*-space). The k_y component of each Bloch wave excitation is conserved at the interface between the PC and exit water medium, leading to several output excitations. Output wave vectors ΓB, ΓC, and ΓD directly relate to input wave vector ΓA. Similarly, output wave vectors ΓB′, ΓC′, and ΓD′ relate to ΓA′. The angles at which the exiting beams leave the back side of the PC are information that provides a fingerprint telling of the angle of the incident acoustic beam that created them.

from the left side of the PC to the right in the same supporting medium (a well-defined volume in the PC). At the interface between the PC and the exit medium, each unique set of Bloch modes in the PC *k*-space translates into a unique set of acoustic wave excitations in the exit medium. In Figure 9, the output acoustic wave vectors ΓB, ΓC, and ΓD directly correlate with the input acoustic wave vector ΓA. Likewise, ΓB′, ΓC′, and ΓD′ are connected to ΓA′. The angles at which the exiting beams leave the back side of the PC are information that provides a fingerprint telling of the angle of the incident acoustic beam that created them. Specifically, output wave vector components directly correlate with input wave vector components. In Figure 9, ΓA enters at +45° and its exit signals, ΓB, ΓC, and ΓD, exit at +45°, −6°, and −62°, respectively. ΓA′ enters at −45° and its exit signals, ΓB′, ΓC′, and ΓD′, exit at +62°, +6°, and −45°, respectively. The splitting of the multiplexed signal into two unique sets of waves (with unique exiting angles) indicates that demultiplexing has occurred at the PC-water interface.

In Figures 10(a) and 10(c), we show with the FDTD method (instantaneous pressure (*P*) calculations) two acoustic sources in water angled at +45° and −45°. The sources, located on the left side of the simulations, launch 590 kHz waves at the epoxy/steel PC surface. The incident beams enter the PC at precisely the same location. In Figures 10(a) and 10(c), the 65 mm mark along the vertical axis marks an axis of symmetry. In Figure 10(a), the sources are set to oscillate π-radians out of phase with each other. In Figure 10(c), the sources oscillate in-phase with each other. In both figures, we observe zero-angle refraction of the input acoustic radiation at the water-PC interface (18 mm mark along horizontal axis in Figures 10(a) and 10(c)). The energy of the two input acoustic waves travels orthogonal to the PC

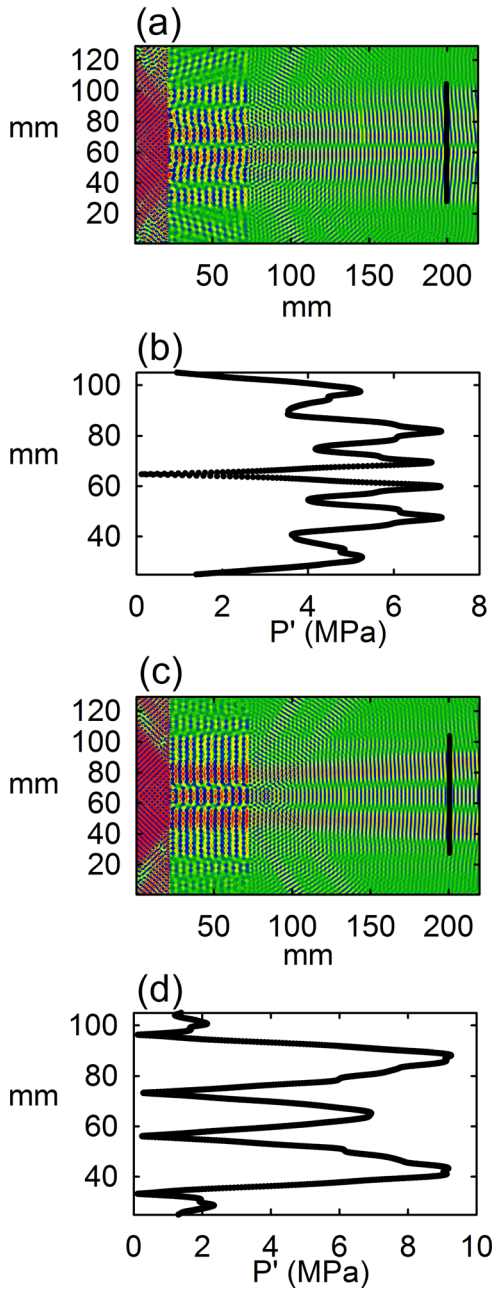

FIG. 10. (a) and (c) FDTD simulation (instantaneous pressure field (P)). Two acoustic waves in water impinge upon the epoxy/steel PC at incidence angles +45° and −45°. The acoustic sources oscillate π radians out-of-phase in (a) and in-phase in (c). Acoustic energy is channeled through the PC. On the backside of the PC, six exiting acoustic waves in water result. The input acoustic wave that enters the PC at +45° separates into a set of three exit beams: {+45°, −6°, and −62°}. The input acoustic wave that enters the PC at −45° separates into a different set of three exit beams: {−45°, +6°, and +62°}. In (b) and (d), surveys of average pressure (P') are presented for the FDTD simulations in (a) and (c), respectively. Average pressure measurements are taken along a line of nodes in the FDTD simulation (black vertical lines in (a) and (c)). Information about the relative phase between the input acoustic sources in (a) and (c) is contained in the magnitude of P' at the 65 mm mark along the vertical axis in plots (b) and (d), respectively.

surface as a multiplexed signal. At the interface between the PC and the exit water medium, as Figure 9 suggests, we observe demultiplexing. The superposed waves inside the PC separate into two distinct sets of exiting acoustic beams on the back side of the PC. The input acoustic wave that

enters the PC at +45° separates into a set of three exit beams: {+45°, −6°, and −62°}. The input acoustic wave that enters the PC at −45° separates into a different set of three exit beams: {−45°, +6°, and +62°}. The angles of the exiting beams connect output acoustic waves to input acoustic waves. For further FDTD analysis, we look at the exiting beams at +6° and −6°. In Figures 10(b) and 10(d), we show plots indicating average pressure (P') cuts taken along a vertical line of nodes in the FDTD grid. These cuts (Figures 10(b) and 10(d)), respectively, correspond to the vertical black lines drawn in Figures 10(a) and 10(c). These plots can be used as acoustic wave detectors. Along the vertical axis in Figures 10(b) and 10(d), average pressure detected at the 45 mm mark and 85 mm mark correspond to the −6° and +6° exiting beams, respectively. For Figure 10(b), we observe two distinct, symmetrical regions of high acoustic pressure. The signal recorded at the 85 mm mark (+6° exiting beam) represents information sent by the −45° input acoustic source. The signal recorded at the 45 mm mark (−6° exiting beam) represents information sent by the +45° input acoustic source. To detail an acoustic wave *k*-space multiplexer, information can be encoded in the amplitude of the +45° and −45° input acoustic waves—wave amplitude is broadcast from each acoustic wave source on the entrance side of the PC to the point of P' detection on the exit side of the PC. We direct the reader to Figure 10(d) to comment on an additional means of encoding information in a set of acoustic signals. Figure 10(d) shows three distinct peaks. As before, the peaks at 45 mm and 85 mm correspond to the −6° and +6° exiting beams, respectively. The central peak, occurring at the axis of symmetry (the 65 mm mark), is telling of constructive interference between the in-phase signals. Wave amplitudes superpose in the region of signal overlap to yield an intense region of acoustic pressure. This central beam can prove to be useful as it details information about the relative phase between the two input acoustic waves. When the input acoustic sources oscillate out-of-phase, as in Figure 10(a), we observe a zero-value reading at the 65 mm mark in Figure 10(b). Oppositely, when input sources oscillate perfectly in-phase, we observe a maximum value reading at the 65 mm mark (Figure 10(d)). The relative phase between the input acoustic beams can be calibrated to the height of the average pressure peak at 65 mm. Thus, with one measurement, the relative phase between the input sources can be identified. The φ-space capabilities of the epoxy/steel PC enable *k*-space multiplexing.

IV. CONCLUSIONS

We have shown that the epoxy/steel PC is multifunctional by operating in ω-space, *k*-space, and φ-space. In comparison to other air/solid or fluid/solid PCs with similar band structure features, the epoxy/steel PC is more practical in terms of device application because it is completely solid. The PC was first shown to behave as a collimator of acoustic wave energy and a device to direct elastic waves in epoxy. φ-space PC capabilities were highlighted with the first ever demonstration of phase-control between propagating acoustic waves via complementary angle inputs in a solid/solid PC. Last, a novel scheme was presented for a *k*-space multiplexer. The work presented here represents a significant effort toward broadening the range of functions associated with PCs. By looking beyond conventional PC capabilities and crossing-over between different PC spaces (ω-space, *k*-space, and φ-space), several new PC functions have been realized.

ACKNOWLEDGMENTS

We gratefully acknowledge the support given by The Chateaubriand Fellowship Program. Additionally, N.S. would like to thank the people at IEMN for their generosity and hospitality.

[1]E. Yablonovitch, Phys. Rev. Lett. **58**, 2059–2062 (1987).
[2]M. M. Sigalas and E. N. Economou, J. Sound Vib. **158**, 377–382 (1992).
[3]M. Sigalas and E. Economou, Solid State Commun. **86**, 141 (1993).
[4]M. S. Kushwaha, P. Halevi, L. Dobrzynski, and B. Djafari-Rouhani, Phys. Rev. Lett. **71**, 2022 (1993).
[5]J. O. Vasseur, P. Deymier, B. Chenni, B. Djafari-Rouhani, L. Dobrzynski, and D. Prevost, Phys. Rev. Lett. **86**, 3012–3015 (2001).
[6]A. Khelif, B. Djafari-Rouhani, J. O. Vasseur, P. A. Deymier, Ph. Lambin, and L. Dobrzynski, Phys. Rev. B **65**, 174308 (2002).
[7]Z. Liu, X. Zhang, Y. Mao, Y. Y. Zhu, Z. Yang, C. T. Chan, and P. Sheng, Science **289**, 1734–1736 (2000).
[8]B. Temelkuran, M. Bayindir, E. Ozbay, R. Biswas, M. M. Sigalas, G. Tuttle, and K. M. Hu, J. Appl. Phys. **87**, 603 (2000).
[9]R. Biswas, E. Ozbay, B. Temelkuran, M. Bayindir, M. M. Sigalas, and K. M. Hu, J. Opt. Soc. Am. B **18**, 1684 (2001).
[10]I. Bulu, H. Caglayan, and E. Ozbay Appl. Phys. Lett. **83**, 3264 (2003).
[11]C. Qiu, Z. Y. Liu, J. Shi, and C. T. Chan, Appl. Phys. Lett. **86**, 224105 (2005).
[12]A. Khelif, P. A. Deymier, B. Djafari-Rouhani, J. O. Vasseur, and L. Dobrzynski, J. Appl. Phys. **94**, 1308–1311 (2003).
[13]S. Yang, J. H. Page, Z. Liu, M. L. Cowan, C. T. Chan, and P. Sheng, Phys. Rev. Lett. **93**, 024301 (2004).
[14]J. B. Pendry, Phys. Rev. Lett. **85**, 3966 (2000).
[15]M. Ke, Z. Liu, C. Qiu, W. Wang, J. Shi, W. Wen, and P. Sheng, Phys. Rev. B **72**, 064306 (2005).
[16]A. Sukhovich, L. Jing, and J. H. Page, Phys. Rev. B **77**, 014301 (2008).
[17]A. Sukhovich, B. Merheb, K. Muralidharan, J. O. Vasseur, Y. Pennec, P. A. Deymier, and J. H. Page, Phys. Rev. Lett. **102**, 154301 (2009).
[18]J. Bucay, E. Roussel, J. O. Vasseur, P. A. Deymier, A.-C. Hladky-Hennion, Y. Pennec, K. Muralidharan, B. Djafari-Rouhani, and B. Dubus, Phys. Rev. B **79**, 214305 (2009).
[19]N. Swinteck, J.-F. Robillard, S. Bringuier, J. Bucay, K. Muralidaran, J. O. Vasseur, K. Runge, and P. A. Deymier, Appl. Phys. Lett. **98**, 103508 (2011).
[20]N. Swinteck, S. Bringuier, J.-F. Robillard, J. O. Vasseur, A. C. Hladky-Hennion, K. Runge, and P. A. Deymier, J. Appl. Phys. **110**, 074507 (2011).
[21]S. Bringuier, N. Swinteck, J. O. Vasseur, J.-F. Robillard, K. Runge, K. Muralidharan, and P. A. Deymier, J. Acoust. Soc. Am. **130**, 1919 (2011).
[22]D. Garcia-Pablos, M. Sigalas, F. R. Montero de Espinosa, M. Torres, M. Kafesaki, and N. Garcia, Phys. Rev. Lett. **84**, 4349 (2000).
[23]G. Mur, IEEE Trans. Electromagn. Compat. **23**, 377 (1981).